Int J Adv Manuf Technol (2014) 74:285–296
DOI 10.1007/s00170-014-5935-z

ORIGINAL ARTICLE

Modeling of transport phenomena and solidification cracking in laser spot bead-on-plate welding of AA6063-T6 alloy. Part II—simulation results and experimental validation

Jiangwei Liu · Zhenghua Rao · Shengming Liao · Pei-Chung Wang

Received: 23 August 2013 / Accepted: 8 May 2014 / Published online: 31 May 2014

Abstract As the mathematical model has been developed in part I, the simulation results of the transport phenomena and solidification cracking in laser spot bead-on-plate welding of AA6063-T6 aluminum alloy and the experimental validation are presented in this paper. Modeling results showed that the solute concentration in the solidified region continuously increases during the solidification process. As the temperature is lower than the coherent temperature (i.e., the temperature at which the coherent mushy zone is just formed), the strains accumulated in the coherent mushy zone increase with the increasing solid fraction. The amount of strain in the mushy zone is primarily determined by the life (i.e., time span) of the coherent mushy zone, which is determined by the solidification range and solidification time. The increased solidification range and consequently solidification time extend the life of the coherent mushy zone, which increases the amount of strain and thus increases the likelihood of solidification cracking. The modeling results are in agreement with the experimental results. Both the experimental and modeling results exhibited that solidification cracking is prone to occurring near the top surface and middle part of the weld bead and an increase of laser power leads to the higher cracking susceptibility.

Keywords Laser welding · Aluminum alloy · Solidification cracking · Mushy zone · Numerical simulation

J. Liu · Z. Rao (✉) · S. Liao
School of Energy Science and Engineering, Central South University, 410083 Changsha, China
e-mail: raoz@csu.edu.cn

P.-C. Wang
Global Research and Development Center, General Motors Corporation, Warren, MI 48090, USA

1 Introduction

In the first part of this study [1], the mathematical model and numerical considerations for the calculations of mass, momentum, heat, species, stresses, and strains during laser spot bead-on-plate welding of aluminum alloy have been developed. In this second part, the simulation results will be presented and validated by the experiments.

Laser welding has been used widely to join metal materials with high precision and efficiency. Despite many advantages over other welding techniques, the use of laser welding of aluminum in vehicle structural applications has been limited, mainly because of concerns regarding the weld discrepancies such as cracking, porosity, and HAZ degradation [2–5]. Solidification cracking is a major discrepancy and commonly observed during laser welding of aluminum alloys if the welding conditions are not set up properly. Previous research [6] indicated that the solidification cracking occurred at the terminal stage of solidification when the metal almost solidified completely with liquid films presented along the grain boundaries. The material becomes very brittle with the existence of liquid films and can be torn apart when the tensile strain is built up. Basically, the controlling factors of solidification cracking consist of metallurgical and mechanical parts [7]. Metallurgical factors include the solidification range, backfilling, dendrite coherency, eutectic fraction, surface tension, grain boundaries, etc. In general, a large solidification range leads to an extended mushy zone and increases solidification cracking susceptibility [8, 9]. Mechanical factors refer to the stresses and strains induced during the solidification process, which provide the driving force to form the cracks. Up until now, various criteria for solidification cracking regarding the behavior of the mushy zone were proposed [10–17]. Since the stress and strain evolutions are closely related to the transport phenomena and material properties, the united modeling of the transport phenomena and

mechanical behavior of the workpiece are essential to predict the solidification cracking.

In comparison with other metals, aluminum alloys are more susceptible to solidification cracking due to its relatively high thermal contraction and solidification shrinkage [5]. Various methods have been proposed to eliminate the solidification cracking during fusion welding of aluminum [18–27]. Cicală et al. [18] made a series of experiments with the attempt to identify the effects of operating factors of laser welding on the weld quality, and the results showed that the most influential factors to the solidification cracking were the welding speed and wire feed rate. The effect of chemical compositions was studied by Kim et al. [19], Ploshikhin et al. [20], and Karunakar et al. [21], and it was found that the cracking was mitigated by adding appropriate amount of some special elements. Ploshikhin et al. [22] investigated the interrelation between the welding parameters, properties of the welded material, and the cracking susceptibility of AA6056-T4 aluminum alloy. It was also reported that the solidification cracking was reduced by introducing a trailing heat sink or an additional heat source in the welding because the mechanical strain in the brittle temperature range (BTR) was reduced by changing the temperature distribution in the material and thus the cooling rates of BTR [23, 24]. Chen and Molian [25] found that solidification cracking was effectively minimized by using the dual beam as compared to single beam laser welding. Zhang et al. [26] investigated the effect the temporal pulse shaping on the solidification cracking susceptibility of Nd:YAG-pulsed laser welds of AA6061-T6 aluminum alloy, and the results showed that the crack-free welds were obtained over a limited range of trailing ramp down gradients. Lakshminarayanan et al. [27] investigated the effect of various fusion welding methods on the strengths of welded AA6061 aluminum alloy and found that the formation of fine, equiaxed microstructure in the weld zone led to the sound weld strength with superior resistance to solidification cracking. However, due to complex phenomena involved in laser welding of aluminum alloys, details of the underlying physics involved in the observed cracking phenomena cannot be fully understood by experiments alone. The united model combining the transport phenomena and stress/strain evolutions for laser welding of aluminum alloys is also not fully developed.

Based on the mathematical model developed in part I of this study, the simulation results of the temperature, velocity, concentration, and stress distributions during laser spot bead-on-plate welding of AA6063-T6 aluminum alloy are presented in this part. The solidification cracking susceptibility is assessed by examining the mechanical strain developed in the coherent mushy zone. The effect of laser power on solidification cracking susceptibility is also discussed in terms of strain accumulation and liquid backfilling in the mushy zone. Finally, the modeling results are validated by the experiments.

2 Results and discussion

Three-millimeter thick AA6063-T6 aluminum alloy was selected in this study. Table 1 lists the physical properties of AA6063-T6 [28]. Note that the absorptivity of laser energy at solid or liquid surface in Table 1 refers to the Fresnel absorption of the incident intensity directly from the laser beam. In fact, once the keyhole is formed, the laser energy is virtually completely absorbed by the keyhole due to multiple reflections, as discussed in part I [1]. Table 2 lists the operating parameters for the laser spot bead-on-plate welding process in the model. A laser beam with a Gaussian distribution is assumed. The workpiece is assumed to be constrained at the sidewalls (r=2.5 mm) and the bottom surface (z=0), which indicates that the normal displacements at these surfaces are set to be zero (see Eqs. (61)–(62) in part I).

2.1 Temperature, velocity, solute, and stress distributions

Modeling results on the sequence of temperature distributions, velocity distributions, solute (Mg_2Si) concentration distributions, and transverse stress distributions for laser spot bead-on-plate welding of 3-mm thick AA6063-T6 at P=3.0 kW are presented in Figs. 1, 2, 3, and 4, respectively. The following phenomena can be observed in the figures: heating and melting of workpiece, weld pool formation and dynamics, formation and collapse of the keyhole, and cooling and solidification of weld metal during laser welding.

Figure 1 shows the temperature distributions in the metal during laser spot bead-on-plate welding of 3-mm thick AA6063-T6 aluminum alloy. As shown, at the beginning of

Table 1 Physical properties of AA6063-T6 aluminum alloy

Nomenclature	Value
Specific heat of solid phase c_s(J/kg–K)	900
Specific heat of liquid phase c_l(J/kg–K)	900
Thermal conductivity of solid phase k_s(W/m–K)	180
Thermal conductivity of solid phase k_l(W/m–K)	180
Density of solid phase ρ_s(kg/m^3)	2,690
Density of liquid phase ρ_s(kg/m^3)	2,690
Dynamic viscosity μ_l(kg/m–s)	0.012
Latent heat of fusion H(J/kg)	3.9×10^5
Initial solidus temperature T_s(K)	888
Initial liquidus temperature T_l(K)	928
Boiling temperature T_v(K)	2,740
Thermal Expansion at 300 K(10^{-6}/K)	27
Absorptivity of laser energy at solid surface	0.2
Absorptivity of laser energy at liquid surface	0.5
Initial solute concentration (Mg) (wt%)	0.7
Initial solute concentration (Si) (wt%)	0.4

Table 2 Process parameters for modeling of laser welding of AA6063-T6 aluminum alloy

Nomenclature	Value
Laser power P (kW)	3.0
Laser beam radius at focus r_{f0}(mm)	0.2
Laser beam radius r_f(mm)	0.2
Substrate initial temperature T_0(K)	300
Surrounding temperature T_{gas}(K)	300
Ambient temperature T_∞(K)	300
Thickness of substrate metal H_b(mm)	3.0
Radius of substrate metal R_b(mm)	2.5
Pulse duration t_d(ms)	18

the welding process (i.e., t<1.6 ms), the laser energy is mainly consumed to heat up the base metal and correspondingly a small weld pool forms. Because the top surface of the workpiece is almost flat at this time, significant laser energy is reflected away [13]. At t=4.8 ms, the laser-induced recoil pressure begins to push the molten metal downward when the liquid metal begins to evaporate, and a keyhole is formed. The temperature of the metal vapor increases quickly, and finally, metal vapor is ionized to form the plasma under the intensive laser beam. The laser-induced plasma has a significant effect on the keyhole drilling process, which absorbs significant laser energy through the iB absorption [13]. This reduces the amount of laser energy that can reach the bottom surface of the weld pool, and consequently, the recoil pressure and drilling speed decrease at the same time. Meanwhile, the hydrostatic pressure at the bottom of the weld pool increases as the keyhole becomes deeper, which provides the higher resistance force to the keyhole drilling process. As a result, the drilling speed gradually decreases during the melting process. Subject to the surface tension and hydrostatic pressure [1], the keyhole begins to collapse when the laser power is shut off at t=18 ms. After that, the temperature of the base metal decreases quickly, and the molten metal is solidified.

Figure 2 presents the corresponding velocity distributions in the weld pool during laser spot bead-on-plate welding of 3-mm thick AA6063-T6. The driving forces are the laser-induced recoil pressure and surface tension force [13]. As shown in Fig. 2, at t=1.6 ms, the melt flow in the weld pool is not significant because of the short action time of recoil pressure. The velocity becomes more significant at t=4.8 ms. At t=8.0 ms, as the keyhole becomes deeper, the metal vapor pulls the liquid at the liquid-gas interface upward. Meanwhile, the recoil pressure is always greater than the hydrostatic pressure during the melting process, and it would squeeze the molten metal to flow upwards. As a result, the molten metal flows outwards and the velocity at the liquid-gas interface is greater than that of the other places of the weld pool. As the keyhole begins to collapse, as shown at t=20.8 ms, the molten metal backfills the keyhole under the hydrostatic pressure. The velocity decreases quickly after the keyhole collapses and disappears gradually during the solidification process.

Figure 3 shows the corresponding solute (Mg_2Si) concentration distributions in the weld metal during laser spot bead-on-plate welding of 3-mm thick AA6063-T6 aluminum alloy. As shown, the initial solute concentration for AA6063-T6 is about 1.083 wt%. From this figure, it is found that the segregation has a significant effect on the solute redistribution. During the melting process at t<14.4 ms, the solute concentration in the weld pool and solid zone is fixed at the initial

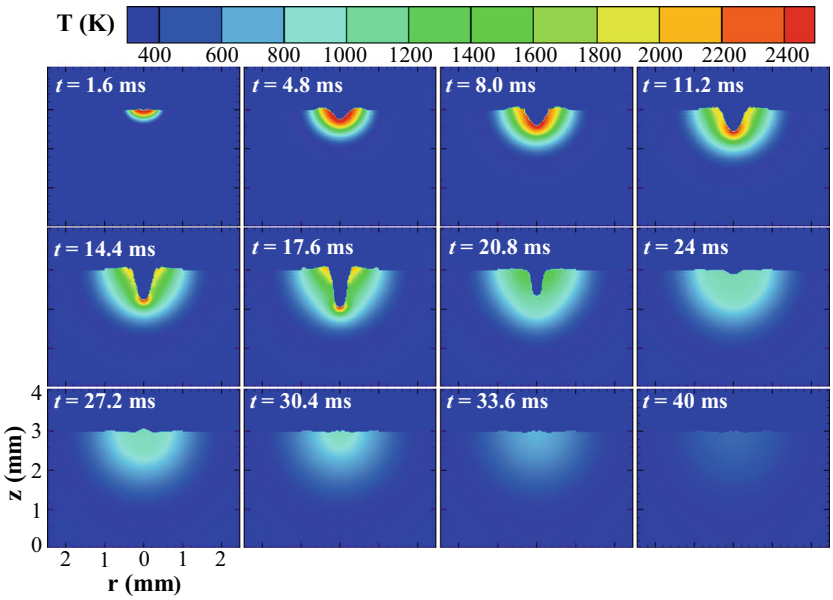

Fig. 1 Temperature distributions in the weld metal for bead-on-plate laser welding of 3-mm thick AA6063-T6 aluminum alloy

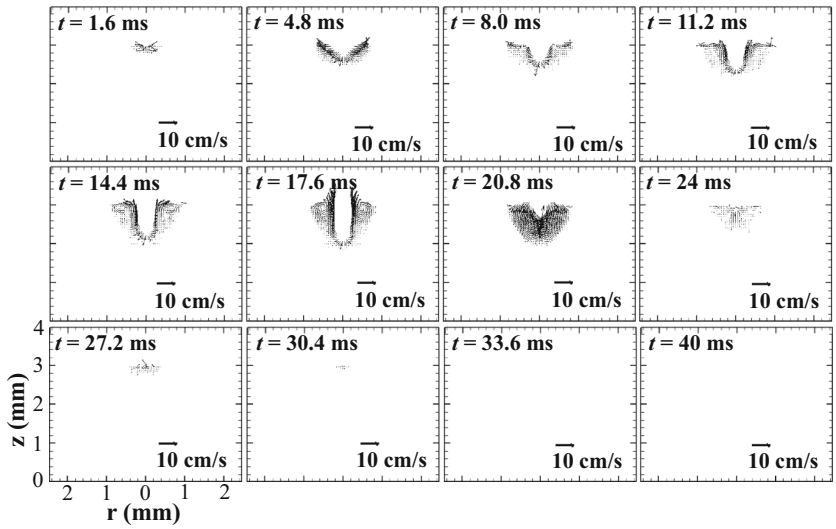

Fig. 2 Velocity distributions in the weld pool for bead-on-plate laser welding of 3-mm thick AA6063-T6 aluminum alloy

concentration because the segregation has not occurred. At t= 14.4 ms, the solute concentration in the solidified region near the top surface begins to decrease, which can be explained as follows. The solidification process is ongoing at the upper boundary of the weld pool at t=14.4 ms while the laser power is still on. This is because most of the laser energy hits at the underside of the keyhole as the keyhole becomes deep. When the keyhole reaches a certain depth, the laser energy received by the upper boundary of the weld pool is less than the heat dissipates to the surroundings, and then the liquid metal begins to solidify at the edge of the weld pool. According to the solidification path prior to the eutectic formation shown in phase diagram (see Fig. 2 in part I), the solute concentration in the solid phase equals to the solute concentration in the liquid phase multiply by the partition coefficient (k_0=0.12) at the solid-liquid interface during solidification. As a result, the solute concentration in the solidified region is quite low at the initial stage due to small partition coefficient. When the laser power is shut off at t=18 ms, the molten metal begins to solidify, and the size of the weld pool decreases quickly. As the liquid metal solidifies, more and more solute is expelled to the weld pool, consequently the solute concentration in the weld pool becomes higher, and correspondingly, the solute concentration in the solidified region continuously increases.

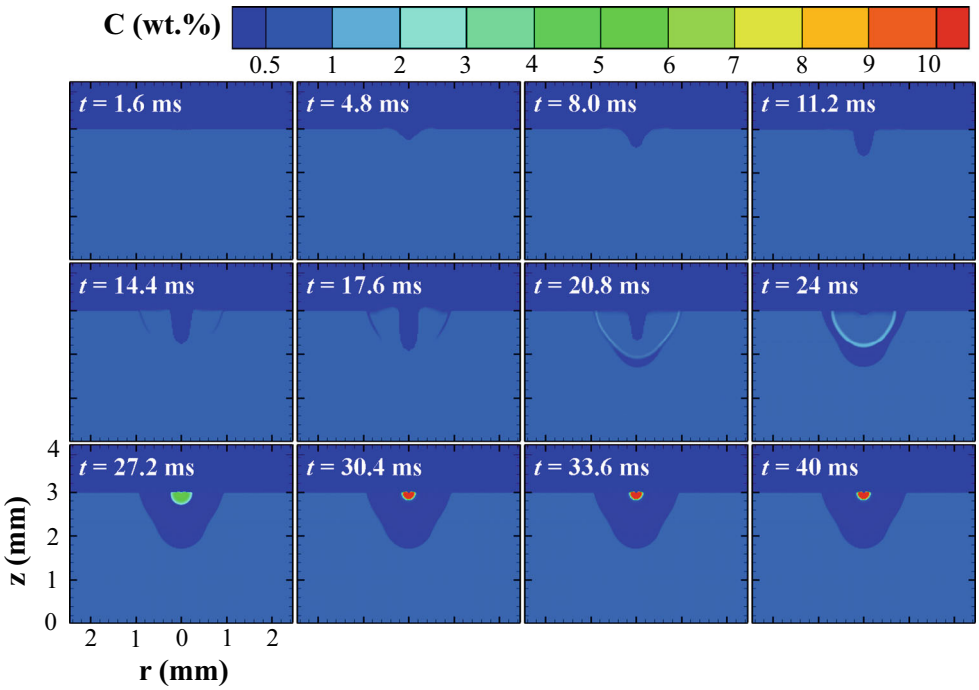

Fig. 3 Concentration distributions in the weld metal for bead-on-plate laser welding of 3-mm thick AA6063-T6 aluminum alloy

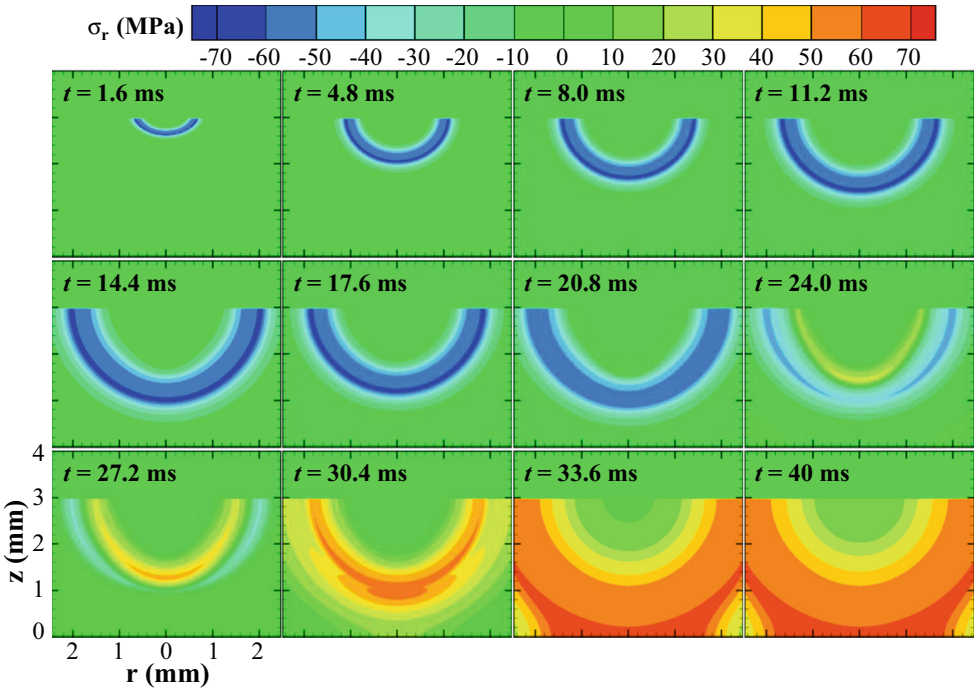

Fig. 4 A sequence of transverse stress distributions in the weld metal for bead-on-plate laser welding of 3 mm thick AA6063-T6 aluminum alloy

As shown, a high concentration zone is observed in the middle portion of the workpiece at the end of solidification.

Figure 4 presents the corresponding transverse stress (i.e., the stress component in the r direction) fields in the workpiece for laser spot bead-on-plate welding of 3-mm thick AA6063-T6 aluminum alloy. Note that the stresses and strains are zero as the temperature is higher than the coherent temperature (i.e., the temperature at which the coherent mushy zone is just formed). As shown, the stresses are negative (i.e., compressive stresses), and the stress distributions have the similar pattern during the whole melting process (t<18 ms). Because the workpiece is constrained at the sidewalls (r=2.5 mm) and the bottom surface (z=0), the thermal expansion occurring in the melting process induces the compressive stresses inside the material. In the zone far away from the weld pool, the magnitude of compressive stress is low because the thermal expansion is quite small due to the insignificant temperature change. The stresses are also very low in the zone near the weld pool in spite of the large thermal expansion. This is because the yield strength of the material is significantly reduced at the elevated temperatures [25]. As a result, a high stress zone is formed in the zone between the above two low stress zones. During the solidification process (t>18 ms), the compressive stresses gradually decrease and the tensile stresses (denoted by the positive values in Fig. 4) gradually build up. For example, the compressive stresses at t=20.8 ms are generally smaller than those at t=18 ms. The tensile stresses are first observed at t=24 ms, which initiate in the solid zone near the weld pool because of a significant decrease in temperature resulting in the large thermal contraction here. Then, the areas under the tension expands, and finally, the whole workpiece is under tensile stresses at t=40 ms. The phenomenon can be explained that the compressive elastic strains caused by aforementioned thermal expansion during the melting are gradually released and the tensile strains gradually developed by the thermal contraction during the solidification process. The evolutions of tensile stresses and strains are critical to the formation of solidification cracking as discussed below.

2.2 Evaluation of solidification cracking

Figure 5 presents the effect of solute segregation on the mechanical strains in the BTR for the regions at z= 2.875 mm of laser spot bead-on-plate welded 3-mm thick AA6063-T6 aluminum alloy. The threshold strain for assessing the cracking occurrence is also given as discussed in part I [1]. In this study, as the temperature reaches the coherent temperature, the mechanical and thermal strains at the coherent solid fraction (f_s=0.6) become zero. The mechanical strains in the BTR increase as the solid fraction increases due to the presence of tensile stresses as f_s>0.6. Since the visco-plastic strains developed in the BTR are time-dependent, the cooling rate becomes the most important factor regarding strain accumulation. The higher cooling rate corresponds to the shorter solidification time within the BTR, which leads to the relatively small visco-plastic strains because the material in the coherent mushy zone has less time to creep. When the segregation is ignored, as shown in Fig. 5a, it is apparent that the mechanical strains become smaller as the

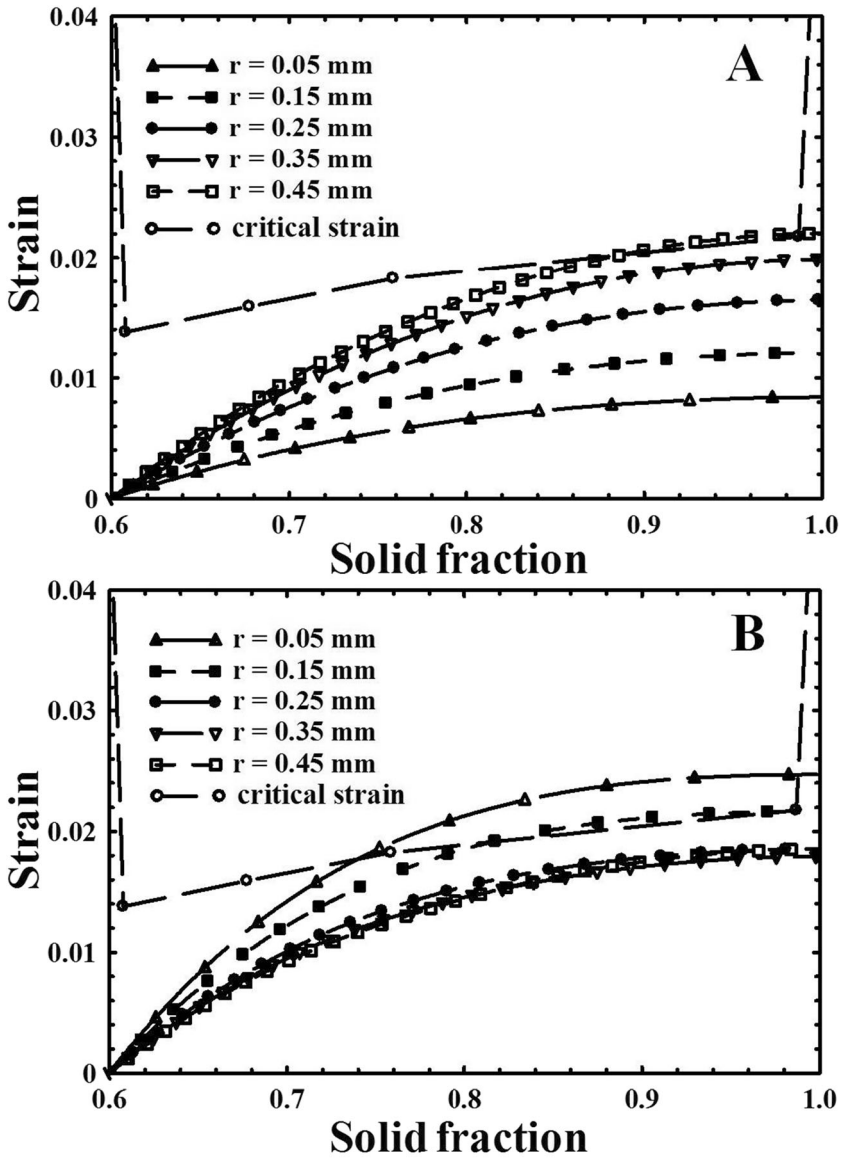

Fig. 5 Effect of segregation on the mechanical strain in the mushy zone at z=2.875 mm for bead-on-plate laser welding of 3-mm thick AA6063-T6 aluminum alloy. **a** without segregation; **b** with segregation

location of the mushy zone gets closer to the central axis of the weld metal. This phenomenon can be further explained as follows. For the case without segregation, the solidification range changes little during the whole solidification process because the solute concentration changes little (C= 1.083 wt%), and consequently, the BTR remains a constant (see Fig. 3 in part I) as the corresponding solid fraction is in the range of 0.6 to 1.0. The cooling rate in the coherent mushy zone is primarily determined by the heating condition of the adjacent weld pool. As the weld pool shrinks and the temperature of the liquid metal decreases in the later stage of the solidification process, the heat dissipation rate from the weld pool to the mushy zone decreases, resulting in a high cooling rate of the coherent mushy zone. Consequently, the accumulated mechanical strains decrease in the region closer to the axis of the weld metal. When the segregation is considered in the solidification process as shown in Fig. 5b, however, the mechanical strains in the region closer to the axis of the workpiece are much higher, as compared to the case without segregation. It is also found that the threshold strain curve within BTR and the strain distribution cross each other at r= 0.05 and 0.15 mm, which indicates the likelihood of solidification cracking near the middle part of the workpiece. For the cases with segregation, the solute concentration in the mushy zone continuously increases during the solidification process, and consequently, the solidification range becomes wider (see Fig. 3 in part I). As a result, the life (i.e., time span) for the coherent mushy zone is longer, leading to the higher mechanical strains. In conclusion, the amount of strain in BTR is primarily determined by the life that the coherent mushy zone experiences, which is determined by the solidification range and weld cooling rate. The

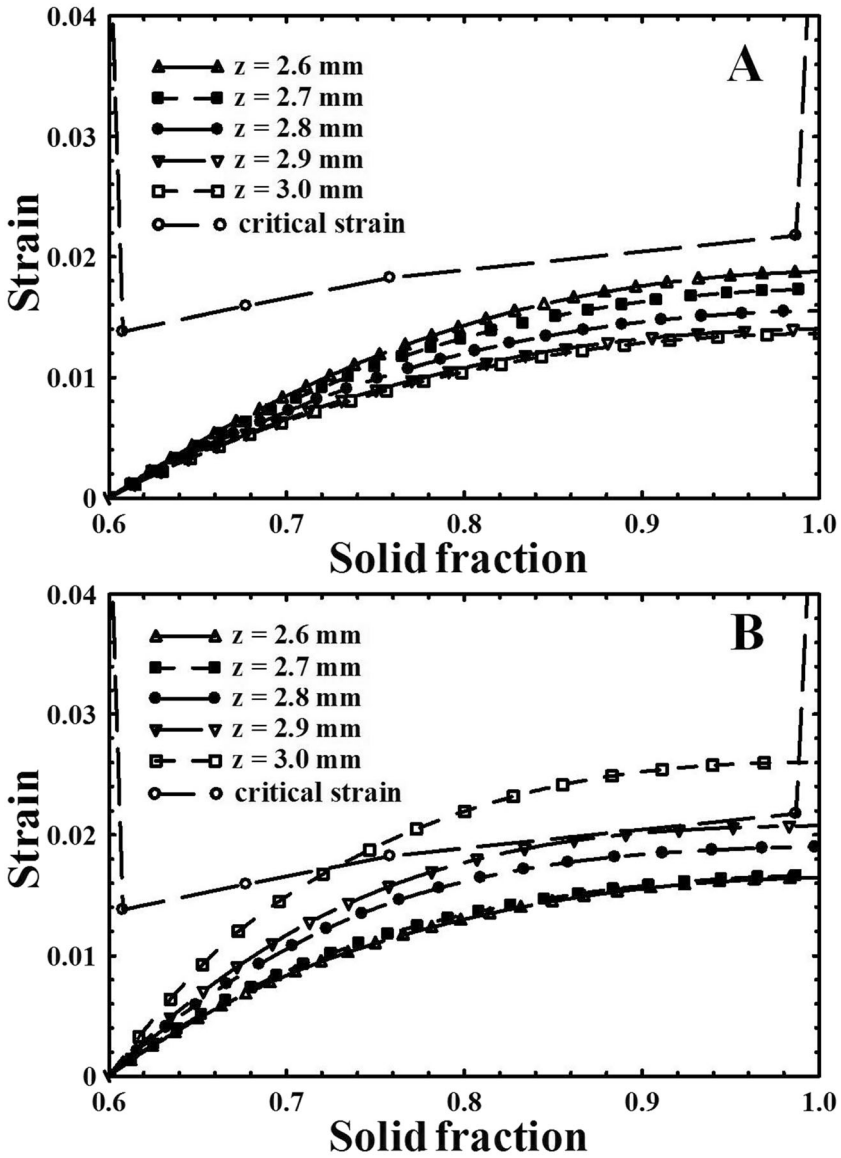

Fig. 6 Effect of solute segregation on the mechanical strain in the mushy zone at r= 0.2 mm for bead-on-plate laser welding of 3-mm thick AA6063-T6 aluminum alloy. **a** without segregation; **b** with segregation

solidification range is mainly dependent on the solute concentration and segregation.

Figure 6 shows the effect of solute segregation on the mechanical strains in the BTR for the regions at r=0.2 mm of laser spot bead-on-plate welded 3-mm thick AA6063-T6 aluminum alloy. As shown, the results for mechanical strains in BTR at r=0.2 mm are similar to the results discussed in Fig. 5. When the segregation is ignored, refer to Fig. 6a, the mechanical strains become smaller as the location of the mushy zone gets closer to the top surface of the weld metal.

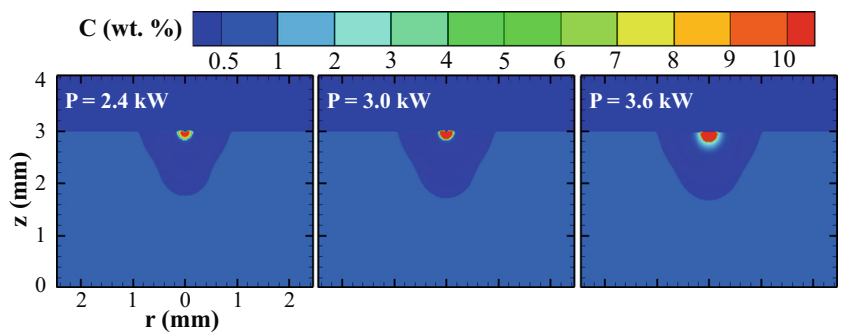

Fig. 7 Effect of laser power on the final solute distribution for bead-on-plate laser welding of 3-mm thick AA6063-T6 aluminum alloy

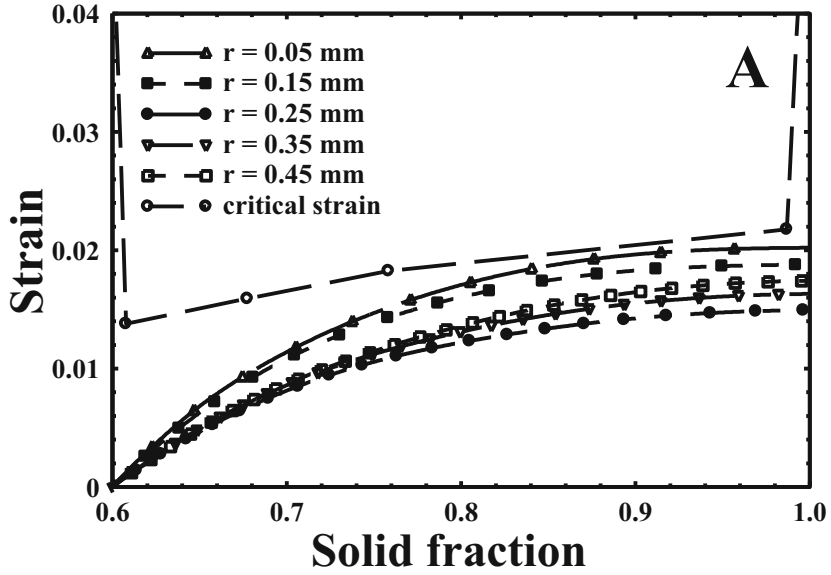
A
r = 0.05 mm
r = 0.15 mm
r = 0.25 mm
r = 0.35 mm
r = 0.45 mm
critical strain
Strain
Solid fraction
0.04
0.03
0.02
0.01
0
0.6
0.7
0.8
0.9
1.0

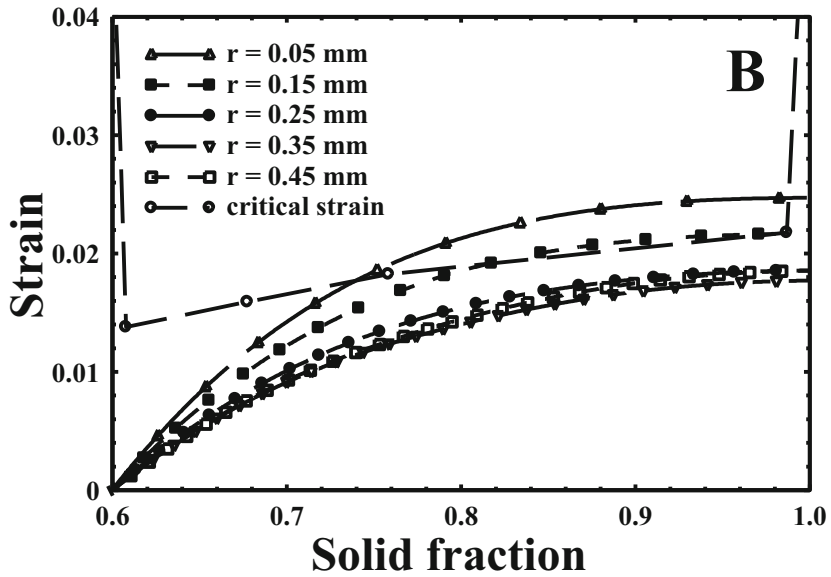
B
r = 0.05 mm
r = 0.15 mm
r = 0.25 mm
r = 0.35 mm
r = 0.45 mm
critical strain
Strain
Solid fraction
0.04
0.03
0.02
0.01
0
0.6
0.7
0.8
0.9
1.0

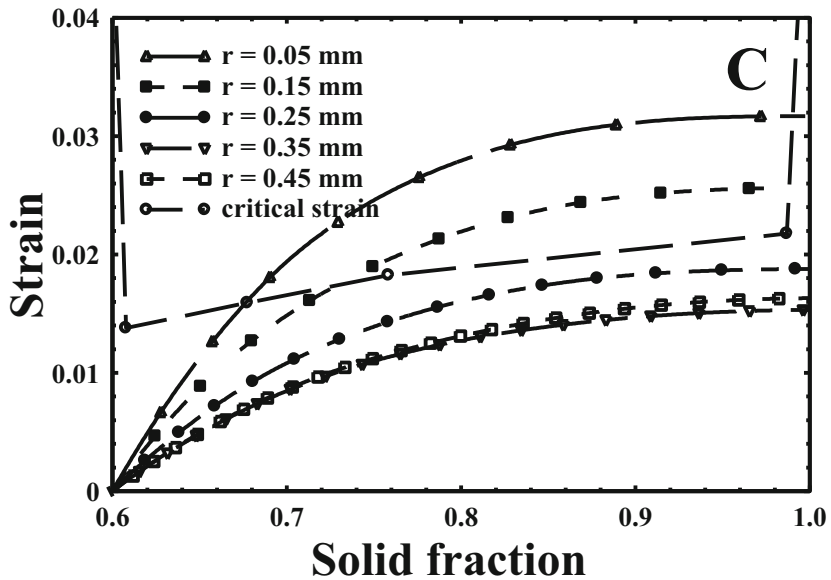
C
r = 0.05 mm
r = 0.15 mm
r = 0.25 mm
r = 0.35 mm
r = 0.45 mm
critical strain
Strain
Solid fraction
0.04
0.03
0.02
0.01
0
0.6
0.7
0.8
0.9
1.0

◀ **Fig. 8** Effect of laser power on the mechanical strains at z=2.875 mm in the mushy zone for bead-on-plate laser welding of 3-mm thick AA6063-T6 aluminum alloy. **a** P=2.4 kW; **b** P=3.0 kW; **c** P=3.6 kW; the segregation is considered

As the segregation is taken into account, refer to Fig. 6b, the region closer to the top surface (z=3.0 mm) has the high strains. This is because the solute concentration in the mushy zone increases during the solidification process, and thus, the solidification range becomes large. As a result, the life for the coherent mushy zone is extended which is helpful for strain accumulation. In turn, as the segregation is considered, the threshold strain curves within BTR and the strains cross each other at z=2.9 and 3 mm, which indicates the high likelihood of solidification cracking near the top surface of the workpiece.

2.3 Effect of laser power

Figure 7 presents the effect of laser power (i.e., P=2.4, 3.0, and 3.6 kW) on the final solute concentration distributions for laser spot bead-on-plate welding of 3-mm thick AA6063-T6 aluminum alloy. As shown, an increase in laser power results in an increase in the weld pool size and consequently the region with the segregation and solute redistribution. From the final solute distribution shown in this figure, it is found that the high solute-concentration zone appears near the center and top surface of the weld bead, and its size increases with the elevation of laser power. This is because the significant amount of solute in the solid metal diffuses into the weld pool during the melting process with an increase in laser power, and thus, the segregation during the solidification process expels the more solute to the end of solidification that is accumulated near the center and top surface. The solute concentration is important for the formation of mechanical strains in the mushy zone and cracking formation as discussed below.

Table 3 Mechanical properties of AA6063-T6 aluminum alloy

Nomenclature	Value
Poisson's ratio	0.33
Elastic Modulus at 300 K (GPa)	68.3
Tensile strength at 300 K (MPa)	241
Yield strength at 300 K (MPa)	214

Figure 8 shows the effect of laser power on the mechanical strains at z=2.875 mm in the mushy zone for laser spot bead-on-plate welding of 3 mm thick AA6063-T6 aluminum alloy. Note that the segregation is considered here. As shown, an increase of laser power leads to an increase in the strains and solidification cracking susceptibility. For example, the threshold strain curve within BTR and the tensile strains cross each other at r=0.05 and 0.15 mm at the laser power levels of P=3.0 and 3.6 kW, which indicates the occurrence of solidification cracking. However, two curves do not cross each other under a laser power of P=2.4 kW, indicating that solidification cracking would not occur. This is mainly because an increase in laser power actually creates a comparatively high-temperature boundary for the mushy zone that would lower its cooling rate and extend the solidification time. Therefore, the high laser power results in a long life for the coherent mushy zone, which increases the amount of mechanical strain and thus the solidification cracking susceptibility.

It should be pointed out that the above discussion about the solidification cracking from Figs. 5, 6, 7, and 8 is based on the strain theory [9]. According to this theory, an increase in mechanical strain developed in the mushy zone leads to an increase in solidification cracking susceptibility. As discussed above, a longer solidification range and a lower cooling rate lead to a longer solidification time that results in higher mechanical strain and solidification cracking susceptibility. However, it has been noticed that the susceptibility of solidification cracking is also related to the liquid backfilling [6]. The solidification cracking occurs only when the mechanical strain exceeds the threshold value and the liquid backfilling is insufficient. Extending the solidification time would allow more time for the liquid metal to backfill, which, in turn, may reduce the solidification cracking susceptibility [26]. As a result, the long solidification time of the coherent mushy zone leads to the different results for the solidification cracking to occur in terms of the accumulated mechanical strains and liquid backfilling. Therefore, there exists a competition between these two conditions. More research remains to be done to decide which conditions, the accumulated mechanical strains in the coherent mushy zone or the liquid backfilling, dominate the occurrence of solidification cracking. Nevertheless, it is significant to evaluate the mechanical strains accumulated in the coherent mush zone as discussed in the present study, which is

Table 4 Chemical compositions of AA6063-T6 aluminum alloy

Chemical composition	Si	Mg	Fe	Cu	Mn	Zn	Cr	Ti	Al
Value (wt%)	0.4	0.7	0.2	0.1	0.15	0.15	0.05	0.1	Balance

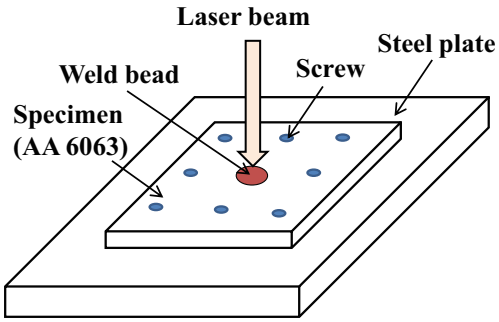

Fig. 9 Schematic of laser spot welding system in the experiment

the necessary condition for the occurrence of the solidification cracking.

3 Experimental validation

3.1 Experimental procedure

3.1.1 Material

Three-millimeter thick AA6063-T6 aluminum alloy was used in the validation experiment. The mechanical properties and chemical compositions of this alloy, per the manufacturer's data sheet, are shown in Tables 3 and 4, respectively.

3.1.2 Sample fabrication

The spot weld configuration, shown in Fig. 9, was selected in this study. The specimens were fabricated from 30×30×3 mm sheets, and a weld was located in the center of each the specimen. In order to constrain the workpieces during welding process, the specimens were constrained by bolted connection on a steel plate as shown in Fig. 9. Prior to welding, the aluminum sheets were degreased by acetone and then polished by abrasive cloth. The YLS-4000-CL fiber laser with the adjustable power of 0–4 kW was used in the experiments. The wavelength and radius of focal point are 1.07 μm and 0.2 mm, respectively. The welding time is 200 ms in this experiment. A 100 % argon with a flow rate of 25 L/min was used as the shielding gas.

3.1.3 Weld examination

To study the quality of laser spot welds and the cracking susceptibility, the top surface and cross-sections of the specimens were prepared and examined. The welds were etched by Dix–Keller's and were examined by FEI Quanta–200 scanning electron microscope.

3.2 Modeling versus experimental results

Figure 10 presents the effect of laser power (i.e., P=3.2 and 3.6 kW) on the cracking susceptibility of a laser spot bead-on-plate welded 3-mm thick AA6063-T6 aluminum alloy. As shown in Fig. 10a, the solidification cracking was found in each case and the cracks were initially developed near the center of the weld bead and propagated outward. This phenomenon is consistent with the aforementioned modeling results. As discussed above, because the segregation leads to wide solidification range in the central part of the weld bead during solidification process, it takes more time for the molten metal at this region to be completely solidified, and

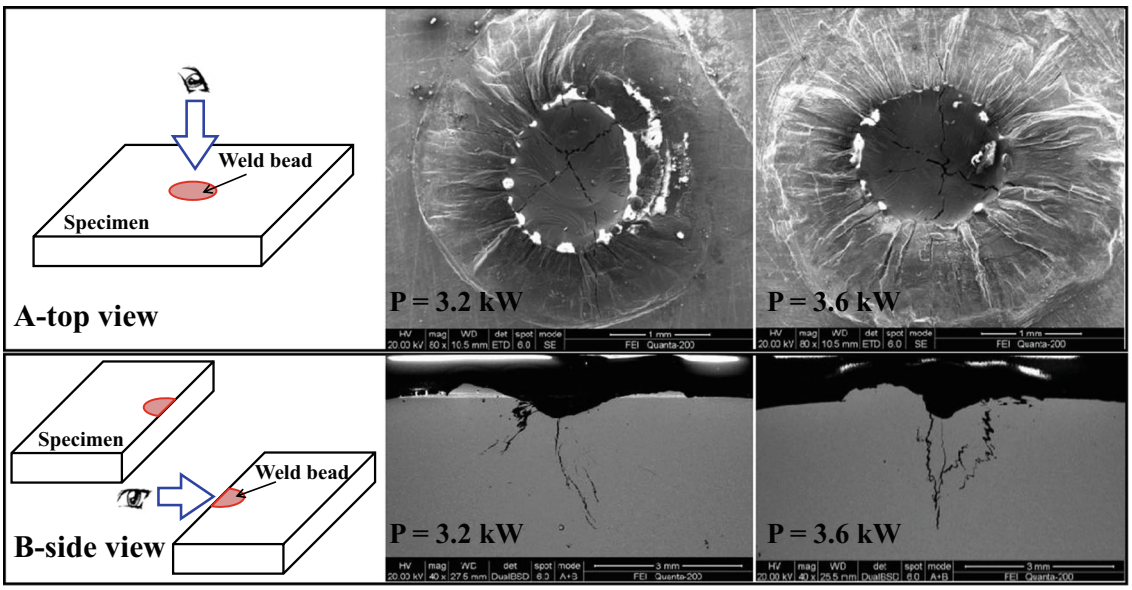

Fig. 10 Effect of laser power on the cracking susceptibility in laser spot welding of 3-mm thick AA6063-T6 aluminum alloy. **a** top view; **b** side view

consequently more mechanical strains are accumulated in the mushy zone. When the accumulated mechanical strain in the mushy zone exceeds the threshold strain, the solidification cracking is likely to occur, and the locations near the middle part become the most sensitive to form the cracking during the solidification process. As comparing these two cases, it was found that the amount and length of the cracks increased as the laser power was increased under a given welding time. These results indicate that the accumulated mechanical strains in the coherent mushy zone prevailed for the occurrence of solidification cracking under the given welding conditions, and an increase in laser power resulted in an increase in susceptibility of the cracking formation, which are in agreement with the modeling results shown in Fig. 8.

As shown in Fig. 10b, the specimens were vertically machined into the two pieces along the center of the weld bead, and cross-section of weld bead was examined from the side view. Test results exhibited that the cracks formed at the region near the center of the weld bead within a range of 1 mm. The cracks initially formed at the top surface of the weld bead and propagated in the workpiece with a depth of about 2 mm. The cracks formed near the top surface of the weld bead in both cases, and they became significant at a laser power of 3.6 kW. These phenomena observed in the experiments are consistent with the modeling results.

It should be pointed out that the quantitative model validation is rather difficult. First, the absorptivity of laser energy at the surface of AA6063-T6 aluminum alloy varies with the temperature while the experimental data are unavailable. In the present calculations, estimated values were used for the absorptivity of solid and liquid surface. Second, the plasma plume above the keyhole attenuates laser propagation through laser absorption, scattering and refraction [2]. Furthermore, it is difficult to create the keyhole at the initial stage due to high reflectivity and cooling effect by shielding gas. All of these details were not included in the modeling. Nevertheless, the present investigation clearly demonstrates the usefulness of the computation model, which can provide the designers with a tool for estimating the effects of aluminum grades and process variables (e.g., laser power and welding time) on the cracking susceptibility of laser spot bead-on-plate welding of aluminum alloys.

4 Conclusions

Based on the mathematical model developed in the first part of this study, the transport phenomena, mechanical behaviors and solidification cracking susceptibility of AA6063-T6 aluminum alloy during laser spot bead-on-plate welding were simulated. Based on the solidification criterion built in first part of this study, the solidification cracking susceptibility of laser spot bead-on-plate welding of AA6063-T6 aluminum was assessed. The modeling results were validated by the experiments. The conclusions are as follows:

1. The mechanical strain at the coherent temperature is zero initially. It increases in the coherent mushy zone as the solid fraction increases during the solidification process. By comparing the calculated mechanical strain with the threshold strain in the coherent mushy zone, it was found that the regions close to the top surface and middle part of the weld bead had a greater tendency to form solidification cracking, which was caused by the higher mechanical strains under the higher solute concentration in the coherent mushy zone. An increase in laser power increases the risk of solidification cracking due to low cooling rate in the coherent mushy zone.
2. The solute segregation is important for the formation of solidification cracking. The amount of mechanical strains accumulated in the mushy zone is determined by the life that the coherent mushy zone experiences, which is a function of the solidification range and weld cooling rate. An increase in solidification range and a decrease in cooling rate extend the life of the coherent mushy zone, which increases the amount of strain and thus results in higher susceptibility for solidification cracking.
3. The modeling results are consistent with the phenomena observed in the experiments. The experimental results confirm that the solidification cracking occurs near the top surface and middle part of the weld bead and an increase in laser power leads to an increase in cracking susceptibility. The results indicate that the solidification-cracking criterion built in this study based on the strain theory can be applied to laser spot bead-on-plate welding of AA6063-T6 aluminum alloy.

Acknowledgement The authors gratefully acknowledge the financial and technical support provided by GM Global Research and Development to carry out the present work.

References

1. Liu JW, Rao ZH, Liao SM, Wang PC (2014) Modeling of transport phenomena and solidification cracking in laser spot bead-on-plate welding of AA6063-T6 alloy. Part I–The mathematical model. Int J Adv Manuf Technol. doi:10.1007/s00170-014-5924-2
2. Mazumder J (1990) Laser–beam welding. In: ASM handbook, volume 6, welding, brazing, and soldering. ASM International, pp. 262–269
3. Kawahito Y, Mizutani M, Katayama S (2007) Elucidation of high-power fiber laser welding phenomena of stainless steel and effect of factors on weld geometry. J Phys D Appl Phys 40:5854–5859
4. Pastor M, Zhao H, Martukanitz RP, DebRoy T (1999) Porosity, underfill and magnesium lose during continuous wave Nd: YAG

laser welding of thin plates of aluminum alloys 5182 and 5754. Weld J 78:207s–216s
5. Zhao H, White DR, DebRoy T (1999) Current issues and problems in laser welding of automotive aluminum alloys. Int Mater Rev 44:238–266
6. Kou S (2003) Solidification and liquation cracking issues in welding. JOM 55:37–42
7. Cross CE (2005) On the origin of weld solidification cracking. In: Böllinghaus T, Herolded H (eds) Hot cracking phenomena in welds, volume 1. Springer
8. Pumphrey WI, Jennings PH (1948) A consideration of the nature of brittleness and temperature above the solidus in castings and welds in aluminum alloys. J Inst Met 75:235–256
9. Pellini WS (1952) Strain theory of hot tearing. Foundry 80:125–199
10. Feurer U (1977) Quality control of engineering alloys and the role of metals science. Delft University of Technology, Delft, pp 131–145
11. Clyne TW, Davies GJ (1979) Comparison between experimental data and theoretical predictions relating to dependence of solidification cracking on composition. In: Solidification and casting of metals. Metals Society, London, 275–278
12. Katgerman L (1982) A mathematical model for hot cracking of aluminum alloys during DC casting. JOM 34:46–49
13. Prokhorov NN (1962) Resistance to hot tearing of cast metals during solidification. Russ Castings Prod 2:172–175
14. Magnin B, Katgerman L, Hannart B (1995) Physical and numerical modelling of thermal stress generation during DC casting of aluminium alloys. In: Cross M., Campbell J (eds) Modeling of casting welding and advanced solidification processes VII. Warrendale, PA, pp. 303–310
15. Braccini M, Martin CL, Suéry M (2000) Relation between the mushy zone rheology and hot tearing phenomena in Al-Cu alloys. In: Sahm PR, Hansen PN, Conley JG (eds) Modeling of casting welding and advanced solidification processes IX. Shaker Verlag, Aachen, pp 18–24
16. Rappaz M, Drezet JM, Gremaud M (1999) A new hot-tearing criterion. Metall Mater Trans A 30:449–455
17. Suyitno, Kool WH, Katgerman L (2005) Hot tearing criteria evaluation for direct-chill casting of an Al-4.5 Pct Cu alloy. Metall Mater Trans A 36A:1537–1546
18. Cicală E, Duffetb G, Andrzejewski H, Grevey D, Ignata S (2005) Hot cracking in Al–Mg–Si alloy laser welding–operating parameters and their effects. Mater Sci Eng A 395:1–9
19. KimHT,NamSW,HwangSH(1996)Studyonthesolidificationcracking behavior of high strength aluminum alloy welds: effects of alloying elements and solidification behaviors. J Mater Sci 31:2859–2864
20. Ploshikhin V, Zoch HW (2005) Integrated mechanical-metallurgical approach to modeling of solidification cracking in welds. Hot Crack Phenom Welds 223–244
21. Karunakar DB, Rai RN, Patra S, Datta GL (2009) Effects of grain refinement and residual elements on hot tearing in aluminum castings. Int J Adv Manuf Technol 45:851–858
22. Ploshikhin V, Prikhodovsky A, Ilin A, Makhutin M, Heimerdinger C, Palm F (2006) Influence of the weld metal chemical composition on the solidification cracking susceptibility of AA6056-T4 alloy. Weld World 50:46–50
23. Yang YP, Dong P, Zhang J, Tian X (2000) A hot-cracking mitigation technique for welding high-strength aluminum alloy. Weld J 79:9–17
24. Hu B, Richardson IM (2006) Mechanism and possible solution for transverse solidification cracking in laser welding of high strength aluminum alloy. Mater Sci Eng A 429:287–294
25. Chen W, Molian P (2008) Dual-beam laser welding of ultra-thin AA 5052-H19 aluminum. Int J Adv Manuf Technol 39:889–897
26. Zhang J, Weckman DC, Zhou Y (2008) Effects of temporal pulse shaping on cracking susceptibility of 6061-T6 aluminum Nd:YAG laser welds. Weld J 87:18–30
27. Lakshminarayanan AK, Balasubramanian V, Elangovan K (2009) Effect of welding processes on tensile properties of AA6061 aluminium alloy joints. Int J Adv Manuf Technol 40: 286–296
28. Davis JR (2010) ASM handbook vol. 02, properties and selection: nonferrous alloys and special-purpose materials, 10th edn. ASM International, Materials Park